Magn Reson Mater Phy (2014) 27:303–316
DOI 10.1007/s10334-013-0412-5

RESEARCH ARTICLE

Quantitative biodistribution and pharmacokinetics of multimodal gadolinium-based nanoparticles for lungs using ultrashort TE MRI

Andrea Bianchi · Sandrine Dufort · François Lux · Arnaud Courtois · Olivier Tillement · Jean-Luc Coll · Yannick Crémillieux

Received: 24 May 2013 / Revised: 9 October 2013 / Accepted: 9 October 2013 / Published online: 30 October 2013

Abstract
Objective To study the biodistribution and lung pharmacokinetics of tracheally administered gadolinium-based contrast agents [gadoteric acid and multimodal ultra-small rigid platforms (USRPs)], to validate their pharmacokinetics against optical imaging of fluorescent USRPs, and to test their short-term toxicity.
Materials and methods Ultrashort echo-time (UTE) lung proton magnetic resonance imaging (MRI) was performed at 4.7-Tesla (T) after the intratracheal instillation of different concentrations of contrast agent solutions in mice. Pharmacokinetic models were implemented on the absolute concentration calculated from the MRI signal enhancement measurements. Fluorescent USRPs were used to obtain optical images with the same protocol. Bronchoalveolar lavage inflammatory cell count and serum creatinine measurement were performed on four groups of instilled mice (sham, saline, USRPs, lipopolysaccharide).
Results MR and optical imaging showed similar kinetics of the USRPs, passing from the airways to the lung tissue and to the kidneys, with negligible hepatic clearance. No significant increase of lung and renal inflammation markers were observed in USRP-instilled animals.
Conclusion A T_1-weighted radial UTE sequence was found to be valuable in quantitatively monitoring the biodistribution and pharmacokinetics of nanoparticles in the lungs of mice. The observed favorable pharmacokinetics, which was validated by fluorescence imaging, ensures the negligible toxicity of the nanoprobes, making the USRPs and the developed protocol good candidates for applications on selected lung diseases.

Keywords Lung · UTE MRI · Gadolinium-based nanoparticles · Fluorescence imaging · Pharmacokinetics · Multimodal nanoparticles

Electronic supplementary material The online version of this article (doi:10.1007/s10334-013-0412-5) contains supplementary material, which is available to authorized users.

A. Bianchi · Y. Crémillieux (✉)
Centre de Résonance Magnétique des Systèmes Biologiques, CNRS UMR 5536, Université Bordeaux Segalen, 146, rue Léo-Saignat (case 93), 33076 Bordeaux, France
e-mail: yannick.cremillieux@u-bordeaux2.fr

A. Bianchi
e-mail: andrea.bianchi@etud.u-bordeaux2.fr

S. Dufort · J.-L. Coll
Université Joseph Fourier, Grenoble, France

S. Dufort
Nano-H, Saint Quentin-Fallavier, France

S. Dufort · J.-L. Coll
INSERM U823, Grenoble, France

F. Lux · O. Tillement
Institut Lumière Matière, CNRS UMR 5306, Université Claude Bernard, Lyon, France

A. Courtois
Centre de Recherche Cardio-Thoracique de Bordeaux, U 1045, Université Bordeaux Segalen, Bordeaux, France

Introduction

In recent years, magnetic resonance imaging (MRI), providing good spatial resolution, high soft tissue contrast and absence of ionizing radiation, has proven to be the most adequate technique for the screening and diagnostics of numerous pathologies in the brain, heart or liver. Nevertheless, this consideration cannot yet be applied to the lung,

which remains one of the most difficult organs to image with MRI because of its intrinsic properties [1–3].

Among the factors that have a negative impact on lung image quality, one can mention (1) the multiple air/tissue interfaces, (2) the low proton density, and (3) the cardio-respiratory motion. However, recent methodological or instrumental developments [1, 4, 5] have somehow circumvented these difficulties in MRI of lung tissue. One efficient strategy relies on the use of ultrashort echo-time (UTE) radial imaging acquisitions [5–8]. UTE techniques applied to lungs have been shown to be very effective for limiting signal losses due to the rapid dephasing of transverse magnetization and for reducing the motion artifacts induced by heart beats and breathing.

In the light of these improvements in lung MRI, several groups have reconsidered the potential of MRI contrast media applied to the lungs [9–12]. The delivery of contrast agents to the lung can be carried out through two main routes: via intravenous injection or via administration to the airways. While the first modality is the most common and easy to implement, the latter presents several advantages, such as direct and local access to the pulmonary tissue, prolonged probe retention and contact with lung tissue, and the exact knowledge of the amount of contrast agent delivered into the pulmonary tract [13–15].

Tracheally administered contrast agents can be used to generate specific contrast mechanisms in the lungs. For instance, as demonstrated previously with aerosols of gadolinium chelates, the changes in signal intensity can be related to the lung ventilation [16, 17]. More importantly, the co-administration of MRI contrast agents associated with drugs or therapeutic nanoparticles can be used for the localization and monitoring of the biodistribution of these therapeutic agents.

In a previous work, Bianchi et al. [12] successfully applied a UTE MRI protocol in mice in order to assess in the lungs the signal enhancement (SE) changes in time after the intratracheal administration of gadolinium-based nanoparticles, and to identify the elimination pathways of the contrast agents. However, the spectrum of information that MRI may offer is much wider and includes, among others, the quantitative evaluation of several pharmacokinetic (PK) parameters that can shed light on a number of aspects relative to the potential diagnostic and therapeutic applications of these nanoassemblies. In addition, the evaluation of the absolute concentration of the theranostic agents in the tissue is of prime importance when therapeutic applications are envisioned.

Given these general objectives, we propose here a UTE MRI study of the biodistribution and pharmacokinetics of two tracheally administered Gd-based contrast agents, namely the widely used gadoteric acid (Dotarem®) and multimodal nanoparticles, hereafter referred to as ultra-small rigid platforms (USRPs). The pharmacokinetics, biodistribution and concentration values of the USRPs were validated against optical imaging of fluorescent USRPs. In relation to the pharmacokinetics of the contrast agents, an acute toxicological study was performed as well, in order to evaluate the short-term toxicity of the USRPs.

Materials and methods

Nanoparticles synthesis and characterization

The USRPs in our study were synthesized according to a previously described protocol [18, 19], slightly modified to obtain higher quantities of nanoparticles. Briefly, they were obtained after a slow dissolution of a gadolinium oxide core, encapsulated in a hollow sphere of polysiloxane, in the presence of a chelating species like DOTA. The resulting nanoparticles were composed of a polysiloxane core surrounded by, on average, ten Gd-DOTA species. When needed to perform optical imaging, Cyanine 5.5 (Cy 5.5) near-infrared dye was covalently grafted onto the nanoparticles (USRPs-Cy 5.5). The detailed description of the synthesis and characterization of the USRPs can be found in the *Supplementary Material*.

The nanoparticles presented with a hydrodynamic diameter of about 4.1 ± 1.0 nm. Due to the small rotation rate, the longitudinal relaxivity r_1 per gadolinium ion was equal to 8.22 $mM^{-1}s^{-1}$ at 4.7T (corresponding to a longitudinal relaxivity of 82.2 $mM^{-1}s^{-1}$ per nanoparticle), roughly three times higher compared to standard Gd-DOTA and Gd-DTPA molecules. The ratio between the transversal relaxivity r_2 and the longitudinal relaxivity r_1 was equal to 1.31. For the fluorescence USRPs, on average, one Cy 5.5 molecule was grafted for every 550 atoms of gadolinium. The half-life of the particles in blood after intravenous injection was found to be equal to 9 min. The hepatic uptake following intravenous injection was measured below 0.15 % of the injected dose through SPECT imaging (after labeling with ^{111}In). More details about the synthesis and the properties of these USRPs can be found in Reference 18.

Animals

For MRI and toxicology experiments, 5-week-old female Balb/c mice ($n = 53$), weighing 24.0 ± 0.5 g, were purchased from Elevage Janvier (Le Genest, Saint Isle, France). For fluorescence experiments, 5-week-old female NMRI nude mice ($n = 11$), weighing 24.0 ± 0.5 g, were purchased from the same rodent breeding company. The use of nude mice for optical imaging allowed us to avoid the typical auto-fluorescence that occurs due to the fur of

Table 1 In vivo experimental design of the study

Bronchoalveolar lavage and creatinine			Histopathological evaluation		
Toxicology					
$n = 4$	Sham	No instillation	$n = 4$	Sham	No instillation (blood, HES)
$n = 4$	Saline NaCl 0.9 %	50 µl bilateral instillation (BAL, blood)	$n = 4$	Saline NaCl 0.9 %	50 µl bilateral instillation (blood, HES)
$n = 4$	USRPs 50 mM Gd^{3+}	50 µl bilateral instillation (BAL, blood)	$n = 4$	USRPs 50 mM Gd^{3+}	50 µl bilateral instillation (blood, HES)
$n = 4$	LPS 0.9 mg/ml	50 µl bilateral instillation (BAL, blood)	$n = 4$	LPS 0.9 mg/ml	50 µl bilateral instillation (blood, HES)
MRI[a]			Fluorescence imaging		
Multimodal imaging					
$n = 3$	10 mM Gd^{3+} USRPs	25 µl selective instillation (PK lung)	$n = 3$	10 mM Gd^{3+} USRPs	25µL selective instillation (PK lung, blood)
$n = 3$	25 mM Gd^{3+} USRPs	25 µl selective instillation (PK lung)	$n = 3$	25 mM Gd^{3+} USRPs	25 µl selective instillation (PK lung, blood)
$n = 3$	50 mM Gd^{3+} USRPs	25 µl selective instillation (PK lung)	$n = 3$	50 mM Gd^{3+} USRPs	25 µl selective instillation (PK lung, blood)
$n = 3$	250 mM Gd^{3+} Dotarem	25 µl selective instillation (PK lung)			
$n = 3$	Saline NaCl 0.9 %	25 µl selective instillation (control)			
$n = 2$	50 mM Gd^{3+} USRPs	50 µl bilateral instillation (Elimination pathways)	$n = 2$	50 mM Gd^{3+} USRPs	50 µl bilateral instillation (Elimination pathways)

[a] MRI preliminary study. 50 µl Dotarem with concentrations: 500 mM, 250 mM, 100 mM, 50 mM Gd^{3+} ($n = 1$/concentration)

Balb/c mice. Before the beginning of the experiment, the animals were acclimatized in a temperature-controlled environment for 1 week. Facility rooms were maintained at a constant temperature (22° C) and humidity (50 % RH), and a 12-h light/12-h dark illumination cycle. Access to food and tap water was available ad libitum. Experiments were carried out following the INSERM (Institut National de la Santé et de la Recherche Médicale) guidelines regarding the fair treatment of animals.

In vivo experimental design

Two separate experiments formed the basis of the in vivo study (Table 1): a pharmacokinetics study through multimodal imaging techniques and an acute toxicological investigation.

Multimodal imaging study

Mice were anesthetized using an intraperitoneal injection of 50 µg/g ketamine (Panpharma, Fougères, France) and 5 µg/g xylazine (Sigma-Aldrich, Saint-Quentin-Fallavier, France). After the acquisition of MR/fluorescence baseline images, an orotracheal intubation was performed on the mice with a 22-gauge Teflon intravenous catheter. The unilateral instillation was performed by passing the catheter through the vocal cords into the beginning of the trachea, before the carina. The catheter was then pushed further into the trachea in order to reach the beginning of the left primary bronchus. The desired volume of contrast agent was introduced in the lungs through the tracheal catheter, allowing diffusion in the left primary bronchus and consequently in the whole (left) lung. The solution of Gd-DOTA-based contrast agent was obtained by dissolving the nanoparticles in saline solution (0.9 % NaCl) to reach the desired concentration.

After the extubation, MR/fluorescence images of the mice lungs were acquired at different times, from 5 min up to 48 h. In the intervals between the acquisitions, animals were extracted from the magnet and left in a temperature-controlled environment where they were allowed to recover. Before the acquisition of the succeeding images, mice were anesthetized with isoflurane at 2 % and repositioned in the magnet using the main anatomic landmarks as reference.

A preliminary study was made in order to evaluate the concentration of commercial gadoteric acid contrast agent (Dotarem®, Guerbet, Villepinte, France) required to reach a SE similar to the one previously shown by the USRPs [12]. Four different concentrations (500, 250, 100 and 50 mM [Gd^{3+}]) of Dotarem® were administered to $n = 4$ mice. The concentration of Dotarem® was then fixed to 250 mM [Gd^{3+}] (See "Results" for explanation) and 25 µl of gadoteric acid were administered to $n = 3$ mice to study

the PK models in the lung (See "Results" for explanation). Similarly, 25 µl of three different USRPs solution concentrations [10, 25 and 50 mM (Gd^{3+})] were administered to different mice ($n = 3$/group) to study the PK models in the lungs. Three control mice received a selective administration of 25 µl of solution 0.9 % NaCl.

For fluorescence imaging, the same three concentrations (10, 25 and 50 mM [Gd^{3+}]; $n = 3$ mice/concentration; USRPs with Cyanine 5.5 grafted onto them) were selectively administered to study the PK in the lungs. We extracted 25 µl of blood from the tail vein before the administration and at different times after (15 min, 30 min, 1, 2, 3, 5, 24 and 48 h). Ten microliters of plasma were obtained after centrifugation of blood (5 min at 3,000 g) and fluorescence imaging was performed on the samples. Finally, $n = 2$ mice received 50 µl of a 50 mM [Gd^{3+}] solution of USRPs-Cy 5.5 in order to verify the elimination pathways also observed with MRI ($n = 2$). Forty-eight hours after the administration of the nanoparticles, all the main organs were extracted and 2D fluorescence imaging was performed.

Acute toxicological study

The toxicological study was performed on two separate sets of $n = 16$ mice (Table 1). Each set was divided into four groups of $n = 4$ mice: (1) a sham group (anesthesia only, without any intratracheal instillation); (2) a negative control group (anesthesia and bilateral intratracheal instillation of 50 µl of saline solution 0.9 % NaCl); (3) a contrast agent group (anesthesia and bilateral intratracheal instillation of 50 µl of 50 mM [Gd^{3+}] USRPs solution); and (4) a positive control group (anesthesia and bilateral intratracheal instillation of 50 µl 0.9 mg/ml of lipopolysaccharide (LPS) *Escherichia coli* Serotype [O111:B4, Sigma Aldrich, Italy)].

Mice were anesthetized using the same procedure as described above and a bilateral orotracheal intubation was performed. The instillation was performed by passing the catheter through the vocal cords into the beginning of the trachea as before, but stopping it before the carina. A volume of 50 µl (saline, USRPs or LPS) was introduced in the lungs through the tracheal catheter, allowing diffusion in both the primary bronchi and consequently in the whole lungs.

On the first set of animals, bronchoalveolar lavage (BAL) and blood were obtained 24 h after the instillation procedure in order to measure the amount of inflammatory cells, total protein count and serum creatinine levels as described below. On the second set of animals, lungs and blood were extracted 24 h after the instillation procedure for histopathology and a second measurement of serum creatinine levels, respectively.

Magnetic resonance imaging

The images were acquired with a 4.7T Biospec 47/50 spectrometer (Bruker, Ettlingen, Germany), using a transmitter/receiver quadrature coil with a 25-mm inner diameter (Bruker, Ettlingen, Germany). The mice were placed prone in a custom-built plastic holder and kept anaesthetized with 2 % isoflurane in a mixture of N_2/O_2 (80:20) via facial mask. The body temperature was kept constant using warm circulating water and the respiratory cycle was monitored constantly, using a pressure sensor placed on the abdomen.

For each animal, six consecutive 1-mm-thick axial slices were acquired in an interleaved scheme to image the lung and the liver. The acquisition was performed in freely breathing animals, using a 2D multislice ultrashort echo time sequence (804 directions/128 points, four averages) with echo time (TE) of 276 µs, repetition time (TR) of 84 ms, bandwidth of 50 kHz, flip angle (FA) of 60° and field of view (FOV) of 3 × 3 cm, according to the optimized protocol of Ref. [12]. The acquisition was preceded by 120 dummy scans. Free induction decay acquisition was started during read gradient ramping, immediately after the Gaussian-shaped RF slice excitation (duration 0.3 ms) and the slice refocusing gradient. The total acquisition time was of about 4 min. Similarly for each animal, ten 1-mm-thick coronal slices were acquired to image the kidneys and the bladder, using a 2D multislice FLASH sequence (matrix size 256 × 256, 1 average) with TE of 2.3 ms, bandwidth of 100 kHz, FA of 60°, FOV of 3 × 6 cm and TR of 100.5 ms for a total acquisition time of about 25 s.

MR images acquired with the UTE sequence were reconstructed with in-house software implemented in IDL (RSI, Boulder, CO). Following the application of a regridding algorithm and a weighting function [20], the images were interpolated to a 256 × 256 image matrix. MR images acquired with the FLASH sequence were reconstructed with the Bruker ParaVision 5.1 software. All the images were saved and analyzed using freeware medical image analysis software (MIPAV by NIH, US-MD).

For each image, the organs of interest were manually segmented to measure the total average signal. The noise of the images was quantified as the standard deviation of the mean signal of a region of interest (ROI) selected in the image background and the signal-to-noise ratio (SNR) was computed. The SE in each image was computed as the difference between the SNR in the lungs after the contrast agent administration and before (baseline images), normalized to the SNR of the baseline images [12, 21]. All the ROIs in the lungs were drawn avoiding the main visible vessels. For each image, the lung (left), kidneys (left and right) and liver were manually segmented. For each mouse, the SE was evaluated on three axial slices (center and

bottom of the lungs and liver) and four coronal slices (two for the kidneys and two for the bladder). For each animal, the SE was averaged over the different measured slices.

For lung UTE images, the absolute concentration of the contrast agent in the parenchyma at the different times was computed from the SE measurement. The mathematical details and the applicability of the procedure are accurately described in the "Appendix".

Briefly, considering that the measured signal follows a well-known signal expression valid for UTE radial sequences [22–24], with straightforward algebraic manipulations, it is possible to compute the longitudinal relaxation time (T_1) value from the measurement of SE. Since the concentration of the contrast agent is related to the T_1 according to the formula $C(t) = 1/r_1 \ [1/T_1(t)–1/T_1(0)]$, knowing the longitudinal relaxivity r_1 of the contrast agent (82.2 $mM^{-1}s^{-1}$ for the USRPs and 3 $mM^{-1}s^{-1}$ for Dotarem® [25]), the absolute concentration of the contrast media in the lung was computed (assuming at 4.7T, $T_1(0) = 1.6$ s for lungs [26]).

Fluorescence imaging

2D-fluorescence images and black-and-white pictures were acquired using a back-thinned CCD camera at −80 °C (ORCAII-BT-512G, Hamamatsu, Massy, France) fitted with a high-pass filter RG9 (Schott, Jena, Germany). Fluorescence images were acquired after illumination with 660-nm light-emitting diodes. Mice were anesthetized (isoflurane 4 %/3.5 % for induction and 2 % thereafter) and the body temperature was kept constant using a warming plate. Image display and analysis were performed using the Wasabi software (Hamamatsu, Massy, France).

For the follow-up of the fluorescence signal in function of time on whole-body images, an ROI was drawn (1) on the lung region and (2) on the skin of the back of each mouse. The number of photons collected into each ROI was then used to calculate the lung/skin ratios. This ratio allowed us to remove the contribution of the skin to the measured fluorescence.

At the end of the experiment, the mice were killed and dissected for imaging organs and plasma. Semi-quantitative data were obtained from the fluorescence images by drawing ROIs on the different organs. The noise was quantified on each image and subtracted from the fluorescence signal. For dissected organs, the results of fluorescence quantifications were expressed as a number of relative light units per pixel per unit of time exposure.

Pharmacokinetic models

An oral instillation model with first-order kinetics was tested on the concentration data to study MRI lung and fluorescence imaging blood clearances, according to the formula:

$$C(t) = A\frac{\tau_d^{-1}}{(\tau_d^{-1}-\tau_e^{-1})}\left(e^{-t/\tau_e} - e^{-t/\tau_d}\right) \quad (1)$$

[27, 28], where τ_d and τ_e indicate the diffusion and elimination time respectively (half-life $= \tau \ln 2$), and A is a free fitting-parameter related to the clearance rate.

All the data fits were performed using Igor Pro 6.2 (WaveMatrics, Inc., Lake Oswego, US-OR).

Bronchoalveolar lavage and creatinine study

Bronchoalveolar lavage was obtained 24 h after the saline/USRPs/LPS intratracheal instillation. Briefly, anaesthetized mice were exsanguinated by cardiac puncture. Blood samples were collected from the right ventricular cavity. Serum was separated by centrifugation at 3,000 g for 10 min at 4 °C, and was analyzed for creatinine concentration according to manufacturer's instructions (Bio-Merieux, Marcy l'Etoile, France).

Mice were placed in the supine position and the trachea was dissected free of connective tissue. A 24-gauge catheter was inserted into the trachea, fixed with a knot, and the lungs were lavaged twice with 0.3 ml of warm NaCl 0.9 %. The BAL samples were gathered and kept on ice until analysis. Total BAL leucocytes were counted under light microscope, and an aliquot (0.1 ml) was sedimented on a glass slide by centrifugation using cytospin® (Cytospin 4, ThermoFisher Scientific, Courtaboeuf, France). Glass slides were dried at room temperature for 30 min, and smears were stained using a Diff-Quick® staining kit (VWR International, Strasbourg, France), adapted from May-Grünwald-Giemsa staining. Differential cell count, i.e., the count of macrophages, eosinophils, neutrophils, and lymphocytes, was performed on each glass slide, in which 400 cells were analyzed by an investigator according to a blinded procedure. The quantity of each cell type was then expressed as cell percentage per ml of BAL. The remaining BAL samples were centrifuged (10 min, 4 °C, 11,000 g) and the supernatants were collected to determine protein concentrations using Biorad protein assay according to manufacturer's instructions (Life Sciences, Marnes-la-Coquette, France).

Histopathological evaluation

Right and left lung tissues were dissected out, fixed with 4 % paraformaldehyde (prepared in phosphate-buffered saline, pH 7.2), and embedded in paraffin. Histological analysis was performed using 4-µm-thick lung slices stained with haematoxylin-eosin-safran (HES). Slices were evaluated by an anatomo-pathologist using light

microscopy. The degree of lung injury was estimated by assigning a semi-quantitative score (0–4) for separate categories representing degenerative, proliferative, and inflammatory alterations, based on incidence, severity and location (bronchial and alveolar). The classification categories included alveolitis, edema, hemorrhage, epithelial desquamation, and peribronchial and perivascular infiltration of both mononuclear cells and granulocytes, according to the protocol developed by Costa et al. [14].

Statistical analysis

Comparison of data between groups for the toxicological data (BAL cells counts, creatinine, protein levels and pathology scores) and PK parameters (diffusion and elimination times for different concentrations) was performed using the Kruskal–Wallis nonparametric test with Dunn's multiple comparison (nonparametric equivalent of the one-way analysis of variance).

Significance was fixed at 5 % probability level. All analyses were performed using GraphPad Prism (GraphPad Software Inc., La Jolla, US-CA). All the data are presented and plotted as mean value ± standard error of the mean (SEM).

Results

MRI imaging

The preliminary study showed that a 250-mM solution of gadoteric acid produces roughly the same SE achievable with a 50-mM [Gd^{3+}] solution of USRPs (319 ± 57 % vs. 294 ± 29 % for 250 mM Dotarem and 50 mM [Gd^{3+}] USRPs solutions, respectively). The concentration of Dotarem® was thus fixed at 250 mM for the following lung PK studies. In Fig. 1, axial slices of the lung before and 45 min after the administration of the different concentrations of USRPs, gadoteric acid or saline solution are shown.

The oral administration one-compartment PK model with first-order kinetics properly fit the concentration of contrast agent measured with MRI in the lungs after intratracheal administration of USRPs or gadoteric acid. In Fig. 2a, the typical data fits for a 250 mM Dotarem® solution and a 50 mM [Gd^{3+}] USRPs solution are shown. The vertical green dashed line highlights the two main regimes taking place in the lungs following the administration of the contrast agent solution. The diffusion regime corresponds to the passage of the paramagnetic contrast agents from the broncho-alveolar space to the lung tissue

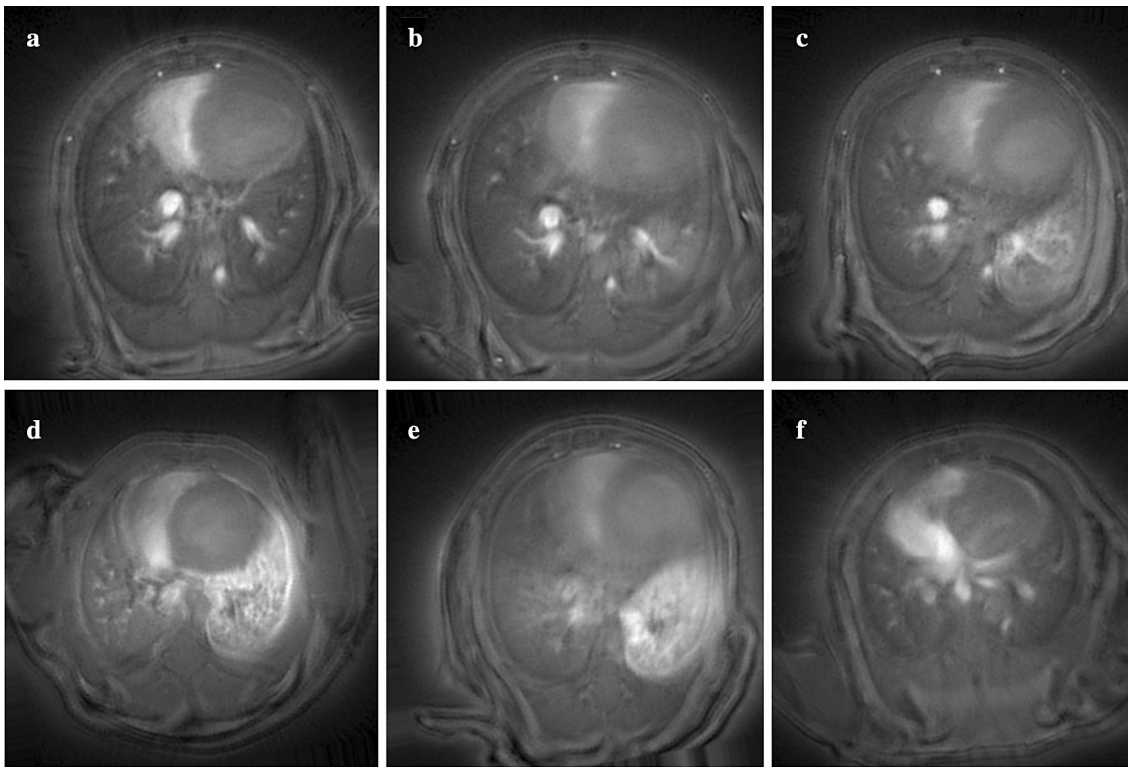

Fig. 1 One of the six UTE axial slices (TE/TR 0.276/84 ms, 804 directions/128 points, four averages, FA = 60°, FOV 3 × 3 cm) of the lung **a** before and 45 min after the selective administration of 25 µl of **b** 10 mM, **c** 25 mM, **d** 50 mM [Gd^{3+}] USRPs solution, **e** 250 mM gadoteric acid or **f** saline solution

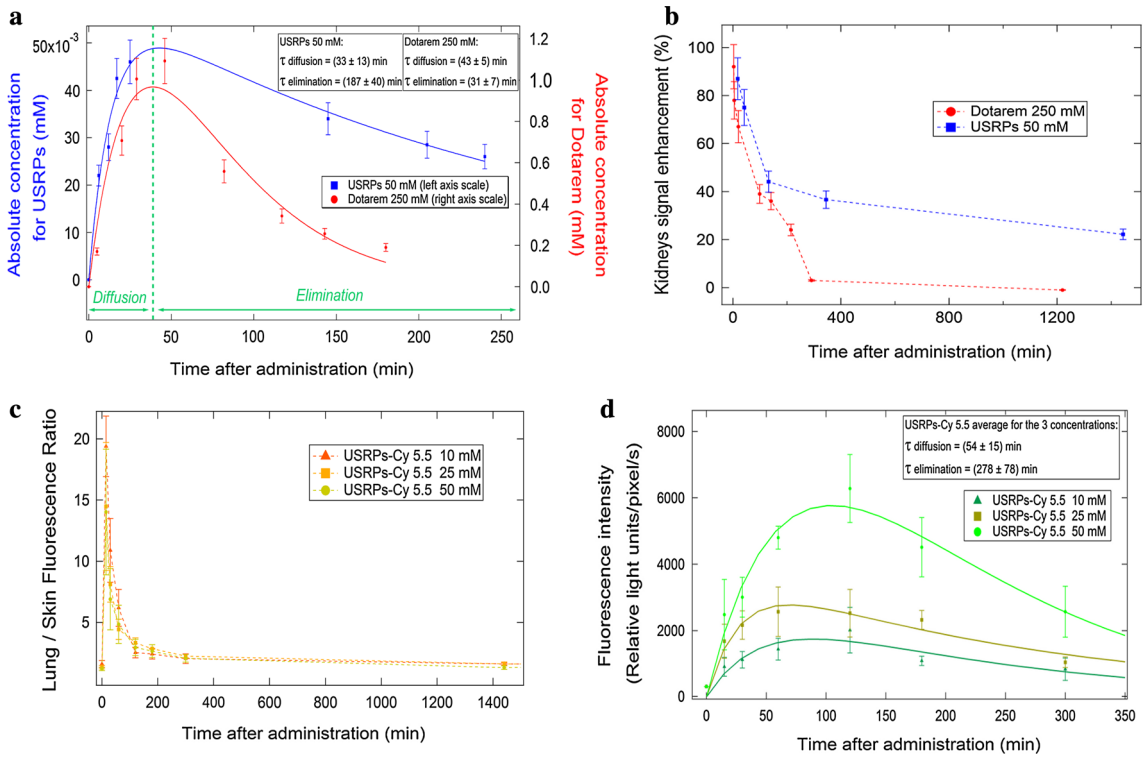

Fig. 2 **a** Typical fit of the computed absolute concentration of the contrast agent in the lungs for a 50-mM USRPs solution (in *blue*, scale on the *left*) and Dotarem® (in *red*, scale on the *right*). The oral administration with first-order kinetics is the PK model that best fit the data. The elimination time constant measured for the USRPs was found to be roughly six times longer compared to the Dotarem® one. **b** Typical data showing the signal enhancement measured in the kidneys for a 50-mM USRPs solution and Dotarem®. The method described to compute the absolute concentration cannot be applied in this case because of the much longer TE of the sequence used to acquire the data (FLASH sequence). For this reason, no PK modeling could be applied to these data. **c** Typical data showing the fluorescence intensity measurements in the lungs for three different concentrations. No fit has been performed since the lung/skin SNR is only semi-quantitative. **d** Typical fit of the fluorescence intensity measurements in the blood for three different concentrations. The oral administration PK model properly fits the data

and blood vessels, whereas the elimination regime corresponds to the diffusion of contrast agents into other body tissues and to their excretion through the kidneys.

No statistically significant concentration-dependence of the USRPs diffusion half-life in the lungs was observed in the explored range, probably due to the low number of animals per group used in the study. Nevertheless, the 50-mM [Gd^{3+}] solution showed an average value three times higher than the 25-mM [Gd^{3+}] and 10-mM [Gd^{3+}] solutions (diffusion time constants for the 50, 25 and 10 mM solutions of 33 ± 13 min, 11 ± 6 min and 9 ± 4 min, respectively, as shown in Fig. 3a). A similar average value was found for the Dotarem® instilled mice (43 ± 5 min). The USPRs showed an elimination half-life in the lungs independent of the solution concentration in the explored range. The average elimination half-life for the three different concentrations was 130 ± 20 min. Such half-life was significantly longer than the one measured for Dotarem® (22 ± 5 min, $p < 0.01$), as shown in Fig. 3b. The maximum value of concentration reached in the lungs after the administration of the USRPs was roughly proportional to the concentration of the instilled nanoparticles, as shown in Fig. 3c. Nevertheless, no statistical difference between the groups was observed, most probably due to the small number of animals per group.

No SE was observed in the liver after the administration of the USRPs. Contrastingly, the nanoparticles rapidly accumulate in the kidneys. At the beginning, the SE quickly decreases (with, on average, a 50 % drop of the SE in about 2 h), then stabilizes (on average, a 50 % drop of the SE in about 22 h), making the contrast agent detectable in the kidneys more than 24 h after the administration, as shown in Fig. 2b. This "two-steps" decay was not observed in the kidney SE curves after intratracheal administration of Dotarem® (with, on average, a 50 % drop of the SE in about 85 min).

Fluorescence imaging

Fluorescence imaging confirmed the elimination pathways observed with MRI, since it showed a fast passage of the nanoparticles in the bloodstream followed by an

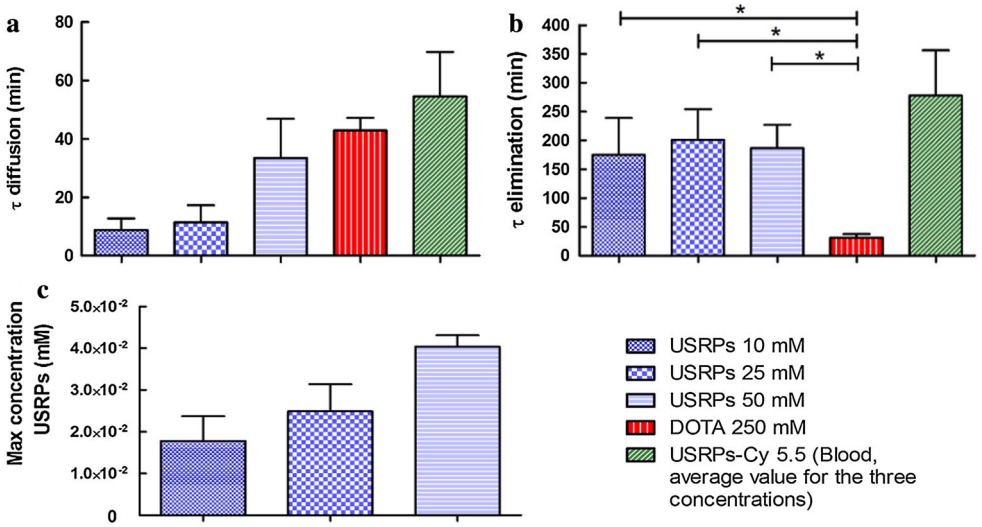

Fig. 3 **a** The diffusion and **b** the elimination time constants obtained from the fit of the lung MRI data and the average one obtained from the fit of fluorescence blood data are shown. **c** The *bar plot* of the maximum concentration measured in the lungs with MRI shows proportionality with the administered concentration of USRPs. The symbol *Asterisk* indicates a probability <0.05

accumulation in the kidneys before the final elimination through urines, as shown in Fig. 4a. No hepatic clearance was observed with optical imaging for the intratracheally-administered USRPs, as visible in Fig. 4b, c.

The maximum of the fluorescence lung/skin SNR curves was observed already at the first measured time point (15 min). The halving of the fluorescence ratio (50 % drop) was visible approximately 2 h after the instillation, even though 24 h after the instillation, the ratio was still slightly above the baseline, as shown in Fig. 2c. No differences were found between the three different concentrations.

The oral administration one-compartment PK model with first-order kinetics properly fit the concentration of contrast agent in the blood measured with fluorescence imaging, as shown in Fig. 2d for the three different concentrations. The USRPs diffusion half-life in the lungs was not statistically different between the three concentrations explored. The average diffusion half-life for the three different concentrations was 38 ± 10 min. This half-life measured in the blood was slightly longer than the one measured in the lungs with MRI (14 ± 6 min, Fig. 2c). The USPRs showed an elimination half-life in the blood independent of the solution concentration in the explored range. The average elimination half-life for the three different concentrations was 193 ± 54 min. This half-life measured in the blood was slightly longer than the one measured in the lungs with MRI (130 ± 20 min, Fig. 2d).

Acute toxicological study

In this set of experiments, BALs were performed in order to study lung injury after intratracheal instillation of USRPs to mice. In BAL, inflammatory cells and protein content were determined in order to assess lung inflammation and the integrity of alveolo-capillary barrier, respectively. As shown in Fig. 5, total cell number and protein concentration in the BAL collected from USRPs-instilled mice were not statistically different from sham or saline-instilled mice. By contrast, animals that received the intratracheal administration of lipopolysaccharide, which was used as a positive control for lung injury, showed a significant increase in the total cell number, in the number of neutrophils, and in protein concentration.

Renal function was assessed through the evaluation of serum creatinine concentrations for the different mice groups [28, 29]. As shown in Fig. 5d, the serum creatinine concentrations from USRPs-instilled mice were not statistically different from the ones measured in sham or saline-instilled mice, whereas they were significantly increased in the LPS-instilled group.

Semi-quantitative histological assessment of the lung sections was conducted using a blinded procedure, relative to exposure. Some accumulation of macrophages was noted in the airway spaces of all the groups. While the control and sham groups showed a low degree of inflammation restricted to the bronchial location, small alveolar injuries were observed in the animals that underwent the USRPs instillation. On the other hand, only the LPS-sensitized mice showed significant epithelial desquamation and occasionally alveolar hemorrhage, with varying degrees of alveolitis characterized by acute neutrophil cell infiltration. Overall, as visible in Fig. 5e, the scoring test showed a non-statistical difference between the control, sham and USRPs-instilled groups.

Discussion

Assuming that the measured MR signal can be described by a well-known signal expression valid for fast imaging

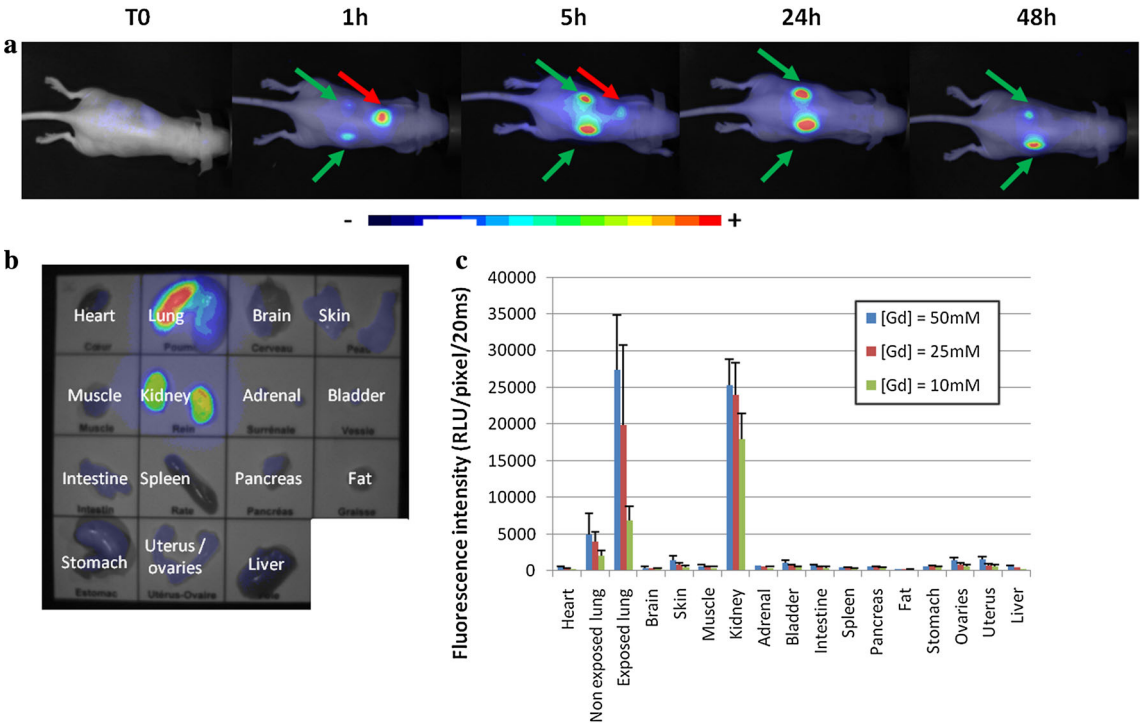

Fig. 4 Biodistribution of USRPs-Cy5.5 nanoparticles after intratracheal administration. **a** 2D-fluorescence images (100 ms integration time) at different times after selective intratracheal instillation of 25 µl of 25 mM [Gd^{3+}] USRPs-Cy5.5 nanoparticles. Fluorescence images are superimposed to visible light images (*black* and *white*). The *red arrow* underline the presence of the nanoparticles in the left lung while the *green* ones put in evidence the accumulation of the USRPs in the kidneys. No fluorescence signal from the bladder is visible in the images since the animals were imaged on their backs; when the mice were imaged on the belly (data not shown in figure), such a signal was clearly identifiable. **b** Example of fluorescence images of isolated organs 48 h after administration of the nanoparticles (25 µl 25 mM [Gd^{3+}] USRPs-Cy5.5, 20-ms integration time). **c** Biodistribution in organs after administration of Cy5.5 nanoparticles at different concentrations 48 h after the instillation. ROIs are defined on the extracted organs in order to semi-quantify the amount of photons detected per pixels after a 20 ms exposure

radial sequences [22–24], in this work we computed the average longitudinal relaxation time and, using the known value of longitudinal relaxivity of the nanoparticles, we showed that it is possible to go back up to the concentration and implement effective quantitative pharmacokinetic models. The developed protocol has allowed us to go beyond the qualitative information previously obtained in Ref. [12], elucidating the timing and elimination kinetics of the used nanoassemblies.

The MRI method developed and implemented to compute the absolute concentration of the contrast agents in the lungs relies on the very short echo time of the UTE sequence and, to the exception of the highest concentrations, the negligible T_2* weighting [22, 24] achieved with the chosen parameters [12]. As a consequence, for the highly concentrated solutions (50 mM [Gd^{3+}] USRPs and 250 mM Dotarem®) the accuracy of this procedure is inferior and may result in the apparent increase in the diffusion time observed, which is actually due to the T_2* effect already observed in [12]. Similarly, the method described in this work cannot be applied to FLASH images because of the much longer echo time of the sequence, which increases significantly the T_2* weighting.

In addition, the employed procedure strongly depends on the constancy of TR before and after the administration of the contrast agent, making mandatory the use of free breathing not-gated acquisitions. The consequent advantages compared to gating techniques, as underlined in Ref. [12], include the shorter acquisition times and the easier protocols, without significant loss in the spatial resolution, signal-to-noise ratio and sharpness [8].

Considering the consistent number of animals involved in this work and the sizeable price of the fluorophore, two slightly different nanoparticles were used to perform MR and optical imaging (USRPs and USRPs-Cy 5.5, respectively). Nevertheless, in agreement with the results presented in Ref. [18], both the nanoparticles showed the same biodistribution and pharmacokinetics, with a fast passage of the USRP solutions from the airways to the lung tissue, then to the kidneys, and finally to the bladder for urine excretion. No significant change in signal intensity was noticed in the liver or spleen, which is in agreement with

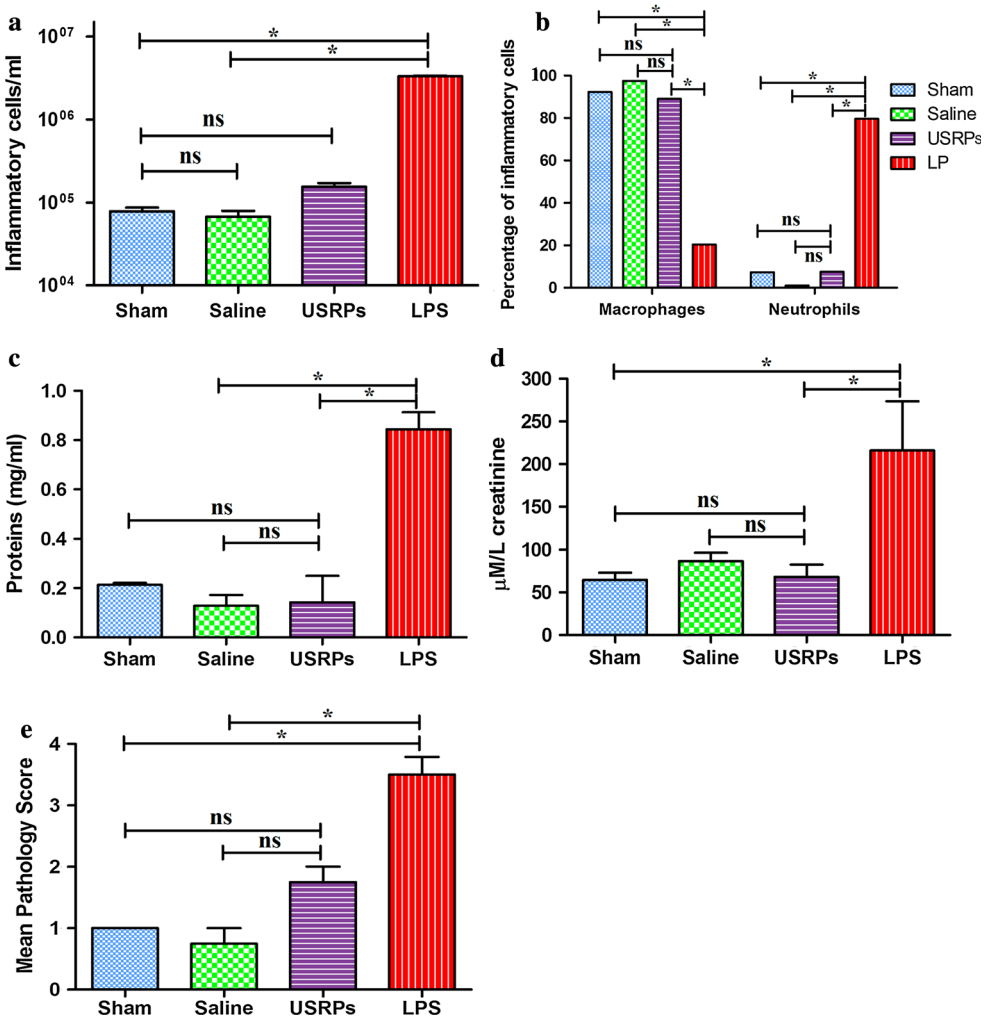

Fig. 5 Results of the bronchoalveolar lavage, blood analysis and histopathological evaluation for the four groups of animals analyzed (sham, saline solution, USRPs and LPS). **a** Inflammatory cell numbers per milliliter of BAL. **b** Differential count (express in %) of BAL inflammatory cells; only macrophages and neutrophils are indicated since the number of lymphocytes and eosinophils was found to be close to zero (<0.5 %) for all the groups. **c** BAL proteins concentrations and **d** serum creatinine concentrations. **e** Semi-quantitative score (0–4) from the histopathological evaluation of bronchial and alveolar degenerative, proliferative, and inflammatory alterations. The symbol *Asterisk* indicates a probability <0.05. "ns" was used to *underline* the non-significant difference ($p > 0.05$) between some groups

the previously reported ability of the USPRs to escape macrophage and monocyte phagocytosis, and with the SPECT measurements presented in Ref. [18]. Such ability has to be attributed mainly to the small dimensions of the hydrodynamic diameter of the employed nanoassembies (<5 nm for both USRPs and USRPs-Cy 5.5), which is the main factor affecting the trafficking across the alveolar surface barrier into tissue and, once there, the biodistribution and clearance of the nanocarriers by the kidneys, as Choi et al. [30] showed with the use of highly sensitive near-infrared fluorescence imaging.

The identification of the mathematical model used to fit and quantitatively describe the data relied on a basic principle in PK studies, according to which the choice of the class of models to be used to describe the observations depends on the number of exponential terms that are needed to describe the whole concentration–time curve [31]. As visible from the concentration–time curves of intratracheally instilled contrast agents, it was clear that at least two regimes were needed to model the data: a diffusion regime and an elimination exponential. Such an observation is in agreement with one of the principles of standard PK studies, which states that when a drug is administered extravascularly (e.g., orally), diffusion into the systemic vascular system must take place before elimination [32]. In this context, the simplest model to be used to fit the data was the one-compartment oral instillation model with first-order kinetics, meaning that the elimination and diffusion of the contrast agent were assumed proportional to the concentration of the contrast medium itself. Fancier models (e.g., the two-compartment oral instillation model) resulted in a poor fit (data not shown) and were therefore discarded.

Modeling the data as described above, the USPRs showed an elimination half-life in the lungs independent of the solution concentration in the explored range, confirming that the excretion mechanisms are not saturated. In addition, the observed linearity of the kinetics, typical of the first-order models [33], ensures that the mathematical model used to study the absolute concentration is a valid choice for the lungs. A similar result was found for the elimination half-lives of the nanoparticles in the blood

through fluorescence imaging. The slightly longer average residence and diffusion time of the USRPs in the blood compared to the lungs can be attributed to the chosen administration modality. After intratracheal instillation, the lung tissue acts as a reservoir of contrast agent: the nanoparticles have to be eliminated from the lung tissue before being completely filtered by the kidneys. Such a peculiar property of the intratracheal administration enables us to prolong the residence time of the studied contrast agent in the blood and might be exploited to increase the accumulation of the nanoparticles in diseased tissues apart from the lungs. Moreover, the presence of the fluorophore grafted onto the USRPs might contribute as well to this slight increase of (1) the diffusion time constant of the nanoparticles from the alveolar space to the lung tissue and blood, and (2) the elimination time-constant of the nanoparticles via the kidneys.

The "two-steps" elimination of the USRPs from the kidneys, which allows detection of a portion of nanoparticles even 24 h after the instillation, can be explained by considering the distribution of sizes of the nanoparticles (4.1 ± 1 nm), with the larger USRPs presumably circulating for a longer time than the smaller ones. Such result was already observed by Lux et al. [18] after intravenous injection of the same gadolinium-based ultra-small nanoassemblies, showing a similar clearance route of the ultra-small nanoparticles disregarding the administration modality.

The faster lung elimination of Dotarem® as compared to USRPs can be related to its smaller hydrodynamic diameter (<1 nm for Dotarem® vs. 4.1 nm for USRPs). This translates into a wider imaging window in lungs for USRPs (sixfold longer residence time in the lungs compared to gadoteric acid) and, as a consequence, a good potential for accumulation in diseased lung tissues.

The fact that the maximum of the SE in the lung observed with fluorescence imaging, contrarily to MRI, was observed right after the instillation (first measured time point) can be explained in light of the intrinsic differences of the signal measured by these two techniques. MRI lung SE arises from the shortening of the spin–lattice relaxation time of lung parenchyma; as a consequence, the enhancement starts to be visible when the nanoparticles pass from the alveolar space into the tissue and blood. Conversely, the signal measured with fluorescence imaging depends on the light re-emission of the stimulated fluorophore Cy 5.5, which does not depend strongly on the interaction of the nanoparticle with the surrounding micro-environment. As a consequence, the enhancement visible with optical imaging reflects the short time needed for the nanoassemblies to distribute in the whole lung airspaces, while the one visible with MRI reflects the time needed for the contrast agent to pass the alveolar barrier and enter the lung tissue. Furthermore, with optical imaging, the nanoparticles are visible in the lungs for a longer time compared to MRI. Such observation clearly reflects the different sensitivity of the two imaging modalities.

Even though the comparison of lung MRI and blood fluorescence measurements with lung optical imaging observations has allowed for validation of the biodistribution and dynamics of the USRPs, the semi-quantitative parameters used for in vivo fluorescence study (lung/skin SNR) does not allow for the implemention of precise PK models. Exploiting the multimodality of the USRPs, a comparison of the absolute concentration measured with MRI and of the one measured with SPECT data can be envisaged (grafting radiolabeled tracers to the USRPs instead of fluorophores [18]) to further validate the obtained results. Although such a measurement goes beyond the purposes of the present work, a quantitative confirmation of the absolute values computed would allow us to corroborate the quantitative method proposed in this work. Since similar ultra-small gadolinium-based nanoparticles have shown a potential theranostic application in brain tumors due to the radio sensitizing effect of the Gd atoms, the accurate knowledge of the absolute concentration of the contrast agent in the healthy and diseased tissues would allow for tailoring of the radiation therapy according to the accumulation effect measurable with MRI, optimizing the theranostic efficacy of these nanoassemblies [34].

It is important to note here that the results and considerations presented in this work are valid independently of the pending assessment of the absolute concentration computations. The time constants used to describe the diffusion and elimination of the contrast media strongly depend on the shape of the time-concentration curves, rather than on the absolute scale. In this sense, a 25 % change in the value of relaxivity hardly affects the observed half-lives (data not shown here), causing just a uniform scaling of the curves and hence only a significant modification of the free parameter A in Eq. (1). Similarly, a change of 10 % of the assumed longitudinal relaxation time of the lung before contrast agent administration results in a change of the presented constants <5 % (data not shown here). On the other hand, the information obtainable from such a parameter (A), which is linked to the clearance rate and bioavailability of the contrast medium [27], is strongly dependent on the assumptions made on the longitudinal relaxivity and on the longitudinal relaxation time of the lungs $T_1(0)$. A confirmation of the absolute concentration measurement would therefore result in a wealth of quantitative data that would further describe the PK of the contrast agents but, at the same time, would require a detailed study of the in vivo variability of r_1 and $T_1(0)$ in order to be reliable.

The elimination pathways observed with complementary imaging techniques, with a negligible retention in the reticuloendothelial system (RES) and an efficient excretion of the unbound material through renal clearance, are good premises for a negligible toxicity of the nanoparticles [35–37]. Nevertheless, a short-term toxicological study was performed to evaluate any possible acute effect due to the chosen administration modality and contrast agent. Such a study was conceived as a basic screening to confirm the hypothesis of non-toxicity formulated after MR- and fluorescence-imaging PK models implementation and was not meant to be an exhaustive test or proof of the absolute safety of the nanoassemblies. Such an investigation, eventually needed before any translational study, goes clearly beyond the purposes of this work.

Altogether, the toxicological study seems to confirm that the intratracheal instillation is a safe way to administer these theranostic nanoparticles in the lungs without causing a significant increase in the number of inflammatory cells or causing any pathological change of the alveolo-capillary barrier. Similarly, no edematous signal was observed in the lungs of the animals that underwent an intratracheal intubation, corroborating the interest in this harmless administration modality that presents several advantages compared to nebulization or intravenous injection [13–15].

In addition, the increase in the total number of inflammatory cells, in the number of neutrophils, and in the morphological pulmonary structure modifications after intratracheal administration of ultra-small gadolinium-DOTA-based nanoparticles were not significant compared to the sham and saline groups, suggesting the negligible acute toxicity of these strongly-chelated assemblies. Contrarily, animals that received LPS, a positive control to induce lung injury [38, 39], showed a significant increase of all the markers of inflammation and alvelo-capillary barrier alteration, in agreement with several previous studies [40, 41].

The absence of difference in the creatinine levels between the negative controls and the USRPs-instilled group ensures that no marked damage of nephrons is caused by the Gd-DOTA-based nanoparticles, in spite of the strong concentrations of the nanoassemblies in the kidneys. The LPS group (used as a positive control [42, 43]), on the contrary, showed a marked increase of the creatinine levels, as expected.

Conclusion

In the present work we have shown that a strongly T_1-weighted radial ultra-short echo time sequence can be used to quantitatively monitor the biodistribution and pharmacokinetics of gadolinium-based nanoparticles in the lungs of freely breathing small animals.

The implementation of pharmacokinetic models in lungs has allowed us to understand the biodistribution, elimination pathways, and timing of the contrast agent. At the same time, the combination of MRI and optical imaging has proven capable of providing complementary synergetic information on the pharmacokinetics and dynamics of the contrast agent.

The observed favorable kinetics of the nanoassemblies, with negligible retention in the RES and effective renal clearance, was confirmed with optical imaging. Such findings ensure the short-term non-toxicity of the contrast agent, as confirmed by the histological analysis. At the same time, the long residence time of the nanoparticles in the lungs and blood, achievable with intratracheal instillation, make the contrast agent and the developed protocol suitable tools for studying the accumulation of the nanoparticles in diseased lung tissues.

The combination of the good spatial resolution and high sensitivity of optical imaging associated with MRI, along with the suitable pharmacokinetics of the nanoparticles and the advantageous instillation procedure, allow us to envisage applications in the diagnosis and investigation of pulmonary pathologies in the near future.

Acknowledgments A.B. acknowledges a fellowship from the European Network PINET (FP7-PEOPLE-2010-ITN-264864). The authors acknowledge the funding support of the Agence Nationale de la Recherche (ANR-12-P2 N-0009) for the ANR project Gd-lung. The authors are grateful to Dr. Gérard Raffard and Dr. Marc Biran for advice and help in use of the MR scanner. They thank Dr. Sylvain Miraux for providing the mouse radiofrequency coil, Dr. Jean-Pierre Labouyrie for help with the creatinine measurements, and Dr. Hugues Begueret and Dr. Olga Ousova for help with the histological studies.

Appendix

The following considerations are valid for a radiofrequency-spoiled sequence, when the pulse duration is negligible compared to T_2^* and the repetition time TR $\geq T_2^*$. Furthermore, it is assumed that in a first approximation the field inhomogeneity and chemical shift can be neglected [23, 24]. Under these assumptions, indicating with α the flip angle, the MRI signal S can be written as:

$$S(t) = \rho\, g \sin\alpha \frac{1 - e^{-TR/T_1(t)}}{1 - \cos\alpha \cdot e^{-TR/T_1(t)}} e^{-TE/T_2^*(t)}, \qquad (2)$$

where ρ indicates the proton density and g the gain of the MR spectrometer.

When a positive contrast agent with relaxivities r_1 and r_2^* is administered at time t at a gadolinium concentration $C(t)$, the inverse of the relaxation times can be expressed using a linear approximation (valid for $C(t) \ll 1$):

$$\frac{1}{T_1(t)} = r_1 C(t) + \frac{1}{T_1(0)}, \frac{1}{T_2^*(t)} = r_2^* C(t) + \frac{1}{T_2^*(0)} \quad (3)$$

Substituting Eq. (3) into Eq. (2), the MR signal in function of time after the administration of contrast agent can be expressed as:

$$S(t) = \rho g \sin\alpha \frac{1 - e^{-\mathrm{TR}/T_1(0) - r_1 C(t) TR}}{1 - \cos\alpha e^{-\mathrm{TR}/T_1(0) - r_1 C(t) TR}} e^{-\mathrm{TE}/T_2^*(0) - r_2^* C(t) \mathrm{TE}} \quad (4)$$

Defining the SE as the difference between the signal before and after the administration of the contrast agent, normalized by the signal before the administration, it is possible to express SE in function of $C(t)$:

$$\begin{aligned} \mathrm{SE}(t) &= \frac{S(t) - S(0)}{S(0)} = \frac{S(t)}{S(0)} - 1 \\ &= e^{-r_2^* C(t) \mathrm{TE}} \times \left[\frac{1 - e^{-A-B} - \cos\alpha(e^{-A} - e^{-2A-B})}{1 - e^{-A} - \cos\alpha(e^{-A-B} - e^{-2A-B})} \right] \\ &\quad - 1, \end{aligned} \quad (5)$$

where $A = \mathrm{TR}/T_1(0)$ and $B = r_1 C(t)$ TR [21]. This formula expresses the relationship between the SE and the contrast agent concentration for different combinations of pulse sequence parameters and MR tissue properties.

If the product r_2^* $C(t)$ TE is small compared to unity ($1/\mathrm{TE} \ll C(t)$ r_2^*, i.e. the T_2^* effect is negligible), the first decay exponential in Eq. (5) (responsible for the T_2^* loss of signal) can be neglected. This condition was shown to be experimentally satisfied by the USRPs for concentrations $\leq$50 mM [Gd^{3+}] for the TE used in the present work with the same UTE sequence [12].

With this approximation, the ratio between the signal after the administration of the contrast agent and the one before, using Eq. (2), can be written as:

$$\begin{aligned} \mathrm{SE} + 1 &= \frac{S(t)}{S(0)} \\ &\cong \left[\frac{1 - e^{-\mathrm{TR}/T_1(t)}}{1 - \cos\alpha e^{-\mathrm{TR}/T_1(t)}} \cdot \frac{1 - \cos\alpha e^{-\mathrm{TR}/T_1(0)}}{1 - e^{-\mathrm{TR}/T_1(0)}} \right] \\ &= \frac{1 - e^{-\mathrm{TR}/T_1(t)}}{1 - \cos\alpha e^{-\mathrm{TR}/T_1(t)}} \cdot \frac{1}{D}, D = \frac{1 - e^{-\mathrm{TR}/T_1(0)}}{1 - \cos\alpha e^{-\mathrm{TR}/T_1(0)}}. \end{aligned}$$

With simple algebraic manipulations, the longitudinal relaxation time after the contrast agent administration can thus be written as a function of the measured SE:

$$T_1(t) = -\mathrm{TR} \Big/ \ln\left[\frac{1 - D(\mathrm{SE} + 1)}{1 - D\cos\alpha(\mathrm{SE} + 1)} \right] \quad (6)$$

Once the $T_1(t)$ has been computed from the SE measurement, the absolute concentration of the contrast agent in the tissue can be inferred using the usual linear relationship:

$$C_{\mathrm{tissue}}(t) = \frac{1}{r_1}\left(\frac{1}{T_1(t)} - \frac{1}{T_1(0)} \right). \quad (7)$$

References

1. Beckmann N, Cannet C, Karmouty-Quintana H, Tigani B, Zurbruegg S, Blé F-X, Crémillieux Y, Trifilieff A (2007) Lung MRI for experimental drug research. Eur J Rad 64:381–396
2. Wielpütz M, Kauczor H-U (2012) MRI of the lung: state of the art. Diagn Interv Radiol 18:344–353
3. Biederer J, Beer M, Hirsch W, Wild J, Fabel M, Puderbach M, Van Beek EJR (2012) MRI of the lung (2/3). Why…when…how? Insights. Imaging 3(4):355–371
4. Mosbah K, Ruiz-Cabello J, Berthezène Y, Crémillieux Y (2008) Aerosols and gaseous contrast agents for magnetic resonance imaging of the lung. Contrast Media Mol Imaging 3:173–190
5. Wild JM, Marshall H, Bock M, Schad LR, Jakob PM, Puderbach M, Molinari F, Van Beek EJR, Biederer J (2012) MRI of the lung (1/3): methods. Insights Imaging 3(4):345–353
6. Bergin CJ, Pauly JM, Macovski A (1991) Lung parenchyma: projection reconstruction MR imaging. Radiology 179:777–781
7. Bergin CJ, Noll DC, Pauly JM, Glover GH, Macovski A (1992) MRI imaging of lung parenchyma: a solution to susceptibility. Radiology 183:673–676
8. Zurek M, Bessaad A, Cieslar K, Crémillieux Y (2010) Validation of simple and robust protocols for high-resolution lung proton MRI in mice. Magn Reson Med 64:401–407
9. Gobbo OL, Zurek M, Tewes F, Ehrhardt C, Crémillieux Y (2012) Manganese: a new contrast agent for lung imaging? Contrast Media Mol Imaging 7:542–546
10. Beckmann N, Kneuer R, Gremlich H-U, Karmouty-Quintana H, Blé F-X, Müller M (2007) In vivo mouse imaging and spectroscopy in drug discovery. NMR Biomed 20:154–185
11. Roller J, Laschke MW, Tschernig T, Schramm R, Veith NT, Thorlacius H, Menger MD (2011) How to Detect a Dwarf. In Vivo Imaging of Nanoparticles in the Lung. Nanomed Nanotechnol Biol Med 7:753–762
12. Bianchi A, Lux F, Tillement O, Crémillieux Y (2012) Contrast enhanced lung MRI in mice using ultra-short echo time radial imaging and intratracheally administrated Gd-DOTA-based nanoparticles. Magn Reson Med. doi:10.1002/mrm.24580
13. Driscoll KE, Costa DL, Hatch G, Henderson R, Oberdorster G, Salem H, Schlesinger RB (2000) Intratracheal instillation as an exposure technique for the evaluation of respiratory tract toxicity: uses and limitations. Toxicol Sci 55:24–35
14. Costa DL, Lehmann JR, Winsett D, Richards J, Ledbetter AD, Dreher KL (2006) Comparative pulmonary toxicological assessment of oil combustion particles following inhalation or instillation exposure. Toxicol Sci 91:237–246
15. Shoyele SA, Cawthome S (2006) Particle engineering techniques for inhaled biopharmaceuticals. Adv Drug Deliv Rev 58:1009–1029
16. Berthezène Y, Vexler V, Clément O, Mühler A, Moseley ME, Brasch RC (1992) Contrast-enhanced MR imaging of the lung: assessments of ventilation and perfusion. Radiology 183:667–672
17. Haage P, Karaagac S, Adam G, Glowinski A, Günther RW (2001) Comparison of aerosolized gadoteridol and gadopentetatedimeglumine for magnetic resonance ventilation imaging of the lung. Magn Reson Med 46:803–806
18. Lux F, Mignot A, Mowat P, Louis C, Dufort S, Bernhard C, Denat F, Boschetti F, Brunet C, Antoine R, Dugourd P, Laurent S, Elst LV, Muller R, Sancey L, Josserand V, Coll J-L, Stupar V, Barbier E, Rémy C, Broisat A, Ghezzi C, Le Duc G, Roux S, Perriat P, Tillement O (2011) Ultrasmall rigid particles as

multimodal probes for medical applications. Angew Chem 123:12507–12511
19. Mignot A, Truillet C, Lux F, Sancey L, Louis C, Denat F, Boschetti F, Bocher L, Gloter A, Stephan O, Antoine R, Dugourd P, Luneau D, Novitchi G, Figueiredo LC, De Morais PC, Bonneviot L, Albela B, Ribot F, Van Lokeren L, Dechamps-Olivier I, Chuburu F, Lemercier G, Villiers C, Marche PN, Le Duc G, Roux S, Tillement O, Perriat P (2013) A top-down synthesis route to ultrasmall multifunctional Gd-based nanoparticles for theranostic applications. Chem Eur J 19:6122–6136
20. Jackson JI, Meyer CH, Nishimura DG, Macovski A (1991) Selection of a convolution function for Fourier inversion using gridding. IEEE Trans Med Imaging 10:473–478
21. Armitage P, Behrenbruch C, Brady M, Moore N (2005) Extracting and visualizing physiological parameters using dynamic contrast-enhanced magnetic resonance imaging of the breast. Med Image Anal 9:315–329
22. Crémillieux Y, Briguet A, Deguin A (1994) Projection-reconstruction methods: fast imaging sequences and data processing. Magn Reson Med 32:23–32
23. Girard OM, Du J, Agemy L, Sugahara KN, Kotamraju VR, Ruoslahti E, Bydder GM, Mattrey F (2011) Optimization of iron oxide nanoparticle detection using ultrashort echo time pulse sequences: comparison of T1, T2*, and synergistic T1-T2* contrast mechanisms. Magn Reson Med 65:1649–1660
24. Strobel K, Hoerr V, Schmid F, Wachsmuth L, Löffler B, Faber C (2012) Early detection of lung inflammation: exploiting T1-effects of iron oxide particles using UTE MRI. Magn Reson Med 68:1924–1931
25. Laurent S, Elst LV, Muller RN (2006) Comparative study of the physicochemical properties of six clinical low molecular weight gadolinium contrast agents. Contrast Media Mol Imaging 1:128–137
26. Zurek M, Alamidi D, Johansson E, Risse F, Olsson LE (2012) Accurate T1 mapping in rodent lungs using ultrashort echo-time MRI. In: proceedings of the 20th scientific meeting. International Society of Magnetic Resonance in Medicine, Melbourne, p 3975
27. Dhillon S, Kostrzewksi A (2006) Clinical Pharmacokinetics. Pharmaceutical Press, London
28. Brenner G, Stevens C (2012) Pharmacology. Saunders Elsevier, Philadelphia
29. Mehta RL, Kellum JA, Shah SV, Molitoris BA, Ronco C, Warnock DG, Levin A, Acute Kidney Injury Network (2007) Acute kidney injury network: report of an initiative to improve outcomes in acute kidney injury. Crit Care 11(2):R31
30. Choi HS, Ashitate Y, Lee JH, Kim SH, Matsui A, Insin N, Bawendi MG, Semmler-Behnke M, Frangioni JV, Tsuda A (2010) Rapid translocation of nanoparticles from the lung airspaces to the body. Nat Biotech 28:1300–1303
31. Wagner JG (1975) Do you need a pharmacokinetic model, and, if so, which one? J Pharmacokinet Biop 3(6):457–478
32. Bauer LA (2005) Clinical pharmacokinetics handbook. McGraw-Hill Medical, New York City
33. Mehvar R (2001) Principles of nonlinear pharmacokinetics. Am J Pharm Educ 65:178–184
34. Le Duc G, Miladi I, Alric C, Mowat P, Bräuer-Krisch E, Bouchet A, Khalil E, Billotey C, Janier M, Lux F, Epicier T, Perriat P, Roux S, Tillement O (2011) Toward an image-guided microbeam radiation therapy using gadolinium-based nanoparticles. ACS Nano 5:9566–9574
35. Choi HS, Liu W, Misra P, Tanaka E, Zimmer JP, Itty Ipe B, Bawendi MG, Frangioni JV (2007) Renal clearance of nanoparticles. Nat Biotech 25:1165–1170
36. Choi HS, Liu W, Liu F, Nasr K, Misra P, Bawendi MG, Frangioni JV (2010) Design considerations for tumour-targeted nanoparticles. Nat Nano 5:42–47
37. Roa WH, Azarmi S, Al-Hallak MK, Finlay WH, Magliocco AM, Löbenberg R (2011) Inhalable nanoparticles, a non-invasive approach to treat lung cancer in a mouse model. J Control Release 150:49–55
38. Tigani B, Schaeublin E, Sugar R, Jackson AD, Fozard JR, Beckmann N (2002) Pulmonary inflammation monitored noninvasively by MRI in freely breathing rats. Biochem Biophys Res Commun 292:216–221
39. Beckmann N, Tigani B, Sugar R, Jackson AD, Jones G, Mazzoni L, Fozard JR (2002) Noninvasive detection of endotoxin-induced mucus hypersecretion in rat lung by MRI. Am J Physiol: Lung C 283:L22–L30
40. Okamoto T, Gohil K, Finkelstein EI, Bove P, Akaike T, van der Vliet A (2004) Multiple contributing roles for NOS2 in LPS-induced acute airway inflammation in mice. Am J Physiol: Lung C 286(1):L198–L209
41. Duan Y, Learoyd J, Meliton AY, Leff AR, Zhu X (2012) Inhibition of Pyk2 blocks lung inflammation and injury in a mouse model of acute lung injury. Respir Res 13:4
42. Zhong F, Chen H, Han L, Jin Y, Wang W (2011) Curcumin attenuates lipopolysaccharide-induced renal inflammation. Biol Pharm Bull 34:226–232
43. Takahashi K, Mizukami H, Kamata K, Inaba W, Kato N, Hibi C, Yagihashi S (2012) Amelioration of acute kidney injury in lipopolysaccharide-induced systemic inflammatory response syndrome by an aldose reductase inhibitor, fidarestat. PLoS ONE 7(1):e30134